



*Original Article*

# Effects of intermediate load on performance limitations in excitation control

Pichai Aree

*Department of Electrical Engineering, Faculty of Engineering,  
Thammasat University, Klong Luang, Pathum Thani, 12121 Thailand.*

Received 14 December 2007; Accepted 22 May 2008

---

## Abstract

The stability of excitation control systems is of great concern in power system operations. In this paper, the effects of intermediate load on performance limitation in excitation control are studied. The results reveal that the open-loop characteristic of synchronous machine's flux linkage can be changed from minimum to non-minimum phase at a high level of intermediate load. This change leads to instability of synchronous machines under manual excitation control. A particular emphasis is also given to investigate the fundamental limitations in excitation control, imposed by non-minimum phases with regard to the open-loop right-half-plane (ORHP) pole. The study demonstrates the difficulties of excitation control tuning to achieve the desired performance and robustness under the ORHP pole occurrence. Moreover, this paper shows the conditional stability in excitation control loop, where either an increase or decrease of the exciter gain causes a destabilization of the system's stability. Frequency response techniques are used for these investigations.

**Keywords:** excitation control, non-minimum phase, performance limitation.

---

## 1. Introduction

Synchronous machines are basic components of power systems. Their steady-state dynamic performances are important (Padiyar, 1995). As most synchronous machines are connected to electrical network systems through transmission lines, a stability analysis of these machines has to be made as they are embedded in the whole system. The stability of synchronous machines under excitation control is a problem that has been widely investigated for a long time (Demello *et al.*, 1969; Kundur, 1993). A suitable designed excitation control can be very efficient to support the voltage on the operation system, to enhance the machine transient performance, and to damp the oscillation (Zhao *et al.*, 1995; Hajagos, 2003).

When the scale of an electric network is expanded with a greater number of synchronous machines and loads, the stabilities of these machines causes concerns in the power

system operations. Because of growth in load, many studies (Crow *et al.*, 1994; Milanovic *et al.*, 1995; Wu *et al.*, 1999; Kao, 2001) have revealed a significant decline of synchronous machine damping. In these papers, the dynamic performance characteristics of synchronous machine under excitation control are studied by both changes in machine loading conditions (increasing or decreasing in grid load) and tie-line impedances. However, a wide range of system operating conditions has not been fully investigated to observe the stability of excitation control as affected by the intermediate load that is placed in the vicinity of the generator. In addition, the dynamic interaction between excitation control and load has not been explored.

In this paper, the instability of excitation control loop, particularly related to the main interaction between the machine's flux linkage and the intermediate load, is investigated in detail. Moreover, the emphasis is given to explore the performance limitations in excitation control, when the internal flux linkage characteristics of synchronous machines are significantly changed from minimum to non-minimum phase at a high level of intermediate load. The limitations in excitation control parameters are also demonstrated under

---

\*Corresponding author.

Email address: [apichai@engr.tu.ac.th](mailto:apichai@engr.tu.ac.th)

non-minimum phase conditions. A frequency response analysis is used in the study

**2. Synchronous machine and load representations**

To gain an insight into the instability of excitation control system with the intermediate load, the three-bus power system shown in Figure 1 is used in this study. It should be noted that since the main objective of this paper is to gain the fundamental knowledge of interaction between synchronous machines and load, the system in Figure 1 is ideal for this kind of study. The system model is derived using differential and algebraic equations of synchronous machines (Arrillaga *et al.*, 1990) and nonlinear voltage-dependent load (IEEE Task Force, 1993). The nonlinear voltage-dependent model is used rather than the induction motor model, since both provide comparable instability (Gebreselassie *et al.*, 1994). The use of the motor model results in lower stability limits. After a suitable deriving process along the same line as Aree (2006), the small-signal transfer functions of the study system are expressed in s domain as follows,

Synchronous generator model:

Swing equations

$$s\Delta\delta = \omega_s\Delta\omega_r \tag{1}$$

$$2Hs\Delta\omega_r = \Delta P_m - \Delta P_e - K_D\Delta\omega_r \tag{2}$$

where,

$$\Delta P_e = K_1\Delta\delta + K_{2d}\Delta E'_d + K_{2q}\Delta E'_q + K_{1G}\Delta G_L + K_{1B}\Delta B_L \tag{3}$$

D-axis flux linkage (field circuit)

$$(1 + K_{3q}\tau'_{do}s)\Delta E'_q = K_{3q}\Delta E_f - K_{4q}\Delta\delta + K_{7q}\Delta E'_d - K_{2G}\Delta G_L + K_{2B}\Delta B_L \tag{4}$$

Q-axis flux linkage (q-axis damper circuit)

$$(1 + K_{3d}\tau'_{qo}s)\Delta E'_d = -K_{4d}\Delta\delta - K_{7d}\Delta E'_q - K_{3G}\Delta G_L - K_{3B}\Delta B_L \tag{5}$$

Generator terminal voltage

$$\Delta E_t = K_5\Delta\delta + K_{6q}\Delta E'_q + K_{6d}\Delta E'_d + K_{4G}\Delta G_L + K_{4B}\Delta B_L \tag{6}$$

Nonlinear voltage-dependent load model:

Load conductance and susceptance

$$\Delta G_L = -(G_L/V_L)(2-n_{ps})\Delta V_L \tag{7}$$

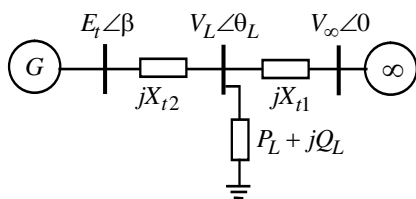


Figure 1. Three-bus power system

$$\Delta B_L = -(B_L/V_L)(2-n_{qs})\Delta V_L \tag{8}$$

Load bus voltage

$$\Delta V_L = K_{v\delta}\Delta\delta + K_{vq}\Delta E'_q - K_{vd}\Delta E'_d - K_{vG}\Delta G_L + K_{vB}\Delta B_L \tag{9}$$

The K-coefficients are listed in Appendix A. By assembling Equations 1-9, the small-signal transfer functions in form of block diagram are displayed in Figure 2.

**3. Interaction between synchronous machine flux linkages and load**

The synchronous machine model inside the dotted-line block in Figure 2 basically consists of shaft dynamics ( $\Delta\delta$  and  $\Delta\omega$ ) and flux linkage dynamics ( $\Delta E'_q$  and  $\Delta E'_d$ ). The nonlinear voltage-dependent load model inside dashed-line block diagram is represented in terms of physical changes of conductance ( $\Delta G_L$ ) and susceptance ( $\Delta B_L$ ). The changes of  $\Delta G_L$  and  $B_L$  directly influence the synchronous machine's dynamics by means of the feedback paths, labeling with A, B, C, and D. The feedback loop gains are dependent on load voltage exponent parameters  $n_{ps}$  and  $n_{qs}$ , and conductance  $G_L$  and susceptance  $B_L$ . By setting  $n_{ps}$  and  $n_{qs}$  to 0, 1, or 2, load is considered as a constant power (P), constant current (I), or constant impedance (Z), respectively. The constant power ( $n_{ps}=n_{qs}=0$ ) has the biggest influence on the machine dynamic characteristics, because the values of loop gains ( $-G_L/V_L$ )( $2-n_{ps}$ ) and  $(-B_L/V_L)(2-n_{qs})$  are highest. The effects of load model parameters on the internal flux linkage  $\Delta E'_q$  of synchronous machine can be demonstrated using the frequency response to explore the open-loop characteristics between the flux

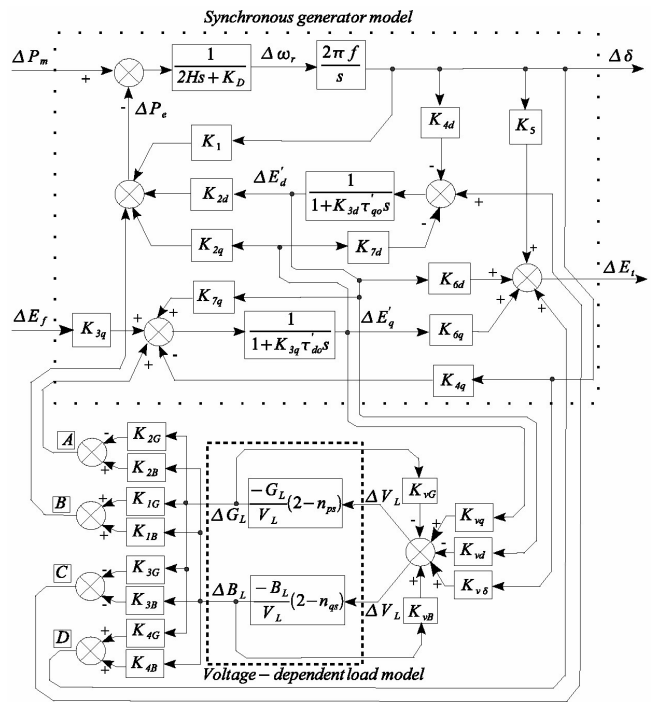


Figure 2. Transfer-function block-diagram model

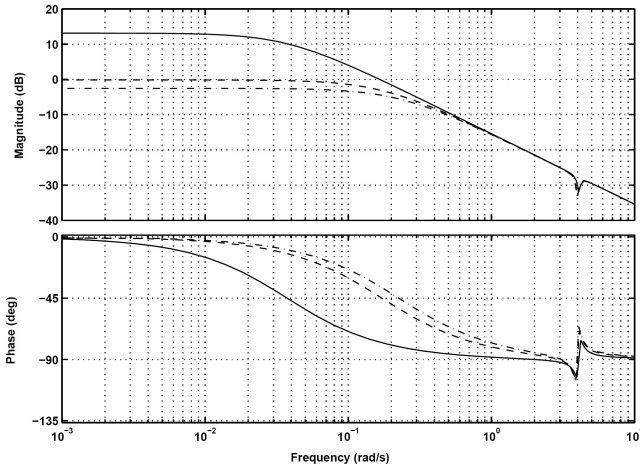


Figure 3. Frequency responses of  $\Delta E'_q/\Delta E_f$  (solid line; constant power, dashed line; constant current, dashed-dotted line; constant impedance)

linkage  $\Delta E'_q$  and excitation voltage  $\Delta E_f$ . The responses are plotted in Figure 3 with three different load model parameters at the same operating conditions. It is evident that the steady-state open-loop gain of the flux linkage channel  $\Delta E'_q/\Delta E_f$  is highest when the constant power load is used. Hence, this load has a great influence on the generator terminal voltage.

#### 4. Stability of excitation control system

In this section, the stability is analyzed, when a synchronous machine is under manual excitation. Manual operation is possible when the machine's field circuit reaches the overexcitation limit. In the study, a 160MVA (MegaVoltAmp) synchronous machine is used with parameters given in Anderson (1993). The synchronous machine shown in Figure 1 is set to export 0.8pu (per unit) (100MVA base) active power to the infinite bus through the interconnected tie line ( $X_{l1}+X_{l2}=0.8$  pu). The load bus is located at 0.3 pu away from the machine terminal bus. The constant power load is used with a fixed power factor (0.8 lagging). The machine and infinite bus voltages are held at 1.0 pu.

To analyze the stability of excitation control loop, the open-loop transfer function between the output terminal voltage ( $\Delta E_t$ ) and the input excitation voltage ( $\Delta E_f$ ) in Figure 2 is employed. This transfer function is closely related to the flux linkage channel ( $\Delta E'_q/\Delta E_f$ ). The studies are conducted by increasing in the intermediate load to the critical level (1.087104 pu), where the system under manual excitation control becomes unstable. The transfer functions with four different levels of active power ( $P_L$ ) of intermediate load are given by Equations 10 to 14.

$P_L = 1.032749$  pu (at 5 % below critical level)

$$\frac{\Delta E_t}{\Delta E_f} = \frac{(s + 0.1701 \pm j4.1795)(s + 3.4396)}{(s + 0.0375)(s + 0.1646 \pm j4.0774)(s + 3.3962)} \quad (10)$$

$P_L = 1.087104$  pu (at critical level)

$$\frac{\Delta E_t}{\Delta E_f} = \frac{(s + 0.1627 \pm j4.1315)(s + 3.4883)}{s(s + 0.1596 \pm j4.0367)(s + 3.4148)} \quad (11)$$

$$\frac{\Delta E'_q}{\Delta E_f} = \frac{(s + 0.1001 \pm j4.0400)(s + 3.4123)}{s(s + 0.1596 \pm j4.0367)(s + 3.4148)} \quad (12)$$

$P_L = 1.141459$  pu (at 5 % above critical level)

$$\frac{\Delta E_t}{\Delta E_f} = \frac{(s + 0.1541 \pm j4.0721)(s + 3.5426)}{(s - 0.0622)(s + 0.1530 \pm j3.9862)(s + 3.4302)} \quad (13)$$

$P_L = 1.195814$  pu (at 10 % above critical level)

$$\frac{\Delta E_t}{\Delta E_f} = \frac{(s + 0.1429 \pm j3.9972)(s + 3.6062)}{(s - 0.1833)(s + 0.1446 \pm j3.9215)(s + 3.4341)} \quad (14)$$

The stability of the excitation control loop can be explored through  $\Delta E_t/\Delta E_f$  using Nyquist diagrams as shown in Figure 4. When  $P_L$  is set at 5 % below the critical level (1.087104 pu), the transfer function of  $\Delta E_t/\Delta E_f$  in Equation 10 indicates that the system has a minimum phase characteristic. In this case, the Nyquist diagram (curve a) makes an encirclement of the  $(-1, j0)$  point in the clockwise direction zero times. Thus, the excitation control loop is stable with open- and close-loop operations. It should be noted that the solid line in the Nyquist diagram is for an oscillation frequency of  $\omega > 0$ , and the dashed line for  $\omega < 0$ . The arrows indicate the direction of movement along the curve with increasing frequency ( $\omega$ ). As  $P_L$  reaches a critical level, the dominant pole of  $\Delta E_t/\Delta E_f$  in Equation 11 is moved to the origin of the  $s$  plane. Therefore, the open-loop gain of  $\Delta E_t/\Delta E_f$  at steady-state conditions is infinite. This result explains the fact that the synchronous machine operating under manual excitation is initially unstable through a monotonic increase or decrease in the terminal voltage  $\Delta E_t$ . At this condition, it is interesting to observe that the open-loop poles of  $\Delta E_t/\Delta E_f$  in Equation 11 are identical to those of  $\Delta E'_q/\Delta E_f$  in Equation 12. This result means that this kind of unstable phenomena is related to the internal instability of the flux linkage  $\Delta E'_q$  due to the impact of load. The dominant open-loop pole in Equation 13 and 14 is moved further into the right-half plane (RHP) as the load is increased above the critical level. Hence, the non-minimum phase characteristic with the negative open-loop gain and unstable ORHP pole appears. Undoubtedly, the system remains unstable. Since the system has one ORHP pole, the Nyquist criterion states that the closed-loop control of the synchronous machine with automatic excitation is stable if and only if the Nyquist plot encircles the  $(-1, j0)$  point one time in the counterclockwise direction. Figure 4 illustrates that the plot (curve b) of  $\Delta E_t/\Delta E_f$  in Equation 13 does indeed encircle the  $(-1, j0)$  point one time. Therefore, if the automatic excitation were incorporated, the closed-loop stability would be obtained because the RHP poles can be displaced into the left-half

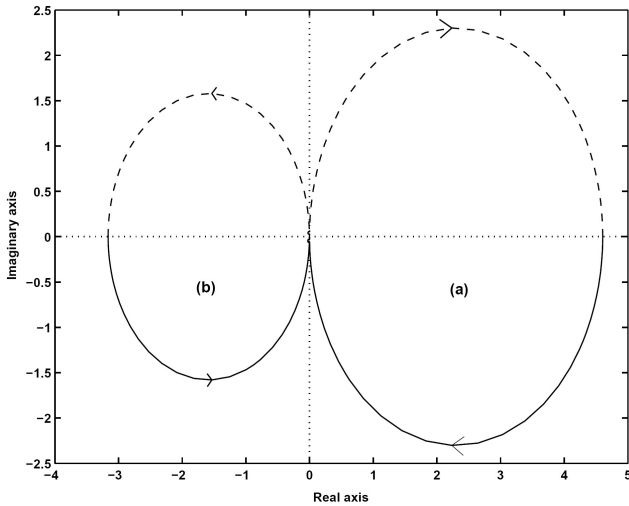


Figure 4. Nyquist responses of  $\Delta E_t/\Delta E_f$  (a;  $P_L = 5\%$  below 1.087104pu, b;  $P_L = 5\%$  above 1.087104pu)

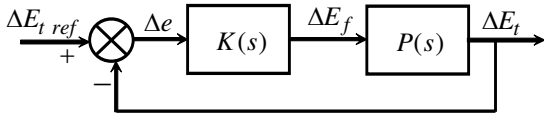


Figure 5. Block diagram of excitation control loop

plane by means of excitation feedback (Huang *et al.*, 1997). This result explains the fact that the system stability margin is increased under automatic excitation control. However, the control performance limitations might occur due to the ORHP pole. These limitations will be discussed in the next section.

**5. Performance limitations in excitation control**

In this section, the performance limitations in feedback of excitation control, caused by the ORHP pole, are investigated using the sensitivity function concept. The sensitivity function  $S(s)$  between the controlled output voltage  $\Delta E_t$ , and the error input signal  $\Delta e$  of the excitation control system in Figure 5 is given by,

$$S(s) = \frac{1}{1 + K(s)P(s)} \tag{15}$$

It is noted that  $P(s)$  is a generator-load transfer function (Figure 2), and  $K(s)$  is an exciter transfer function. The plots of sensitivity functions are displayed in Figure 6. Under manual excitation without  $K(s)$ , the value of the sensitivity function (dotted line) is small in the low-frequency region. As the load is increased above the critical level, the value of the low-frequency sensitivity function increases significantly with regard to the movement of the open-loop pole into the right-half plane, indicating that disturbance amplification occurs. Consequently, it is difficult to achieve a disturbance rejection and closed-loop stabilization. On the other hand,

when the automatic excitation control is incorporated, with a gain of  $K_a=20$  and a time constant of  $\tau_a=0.5\text{sec}$ , the amplitude of the sensitivity function (solid line) is getting smaller, particularly in the low-frequency region. However, the sensitivity function is increased with a peaking phenomenon at other frequencies at 4 rad/sec. This result indicates that the disturbance attenuation is improved in one frequency range, but gets worse in others. If the disturbance comes in with energy close to this concerned frequency, it will be greatly amplified. This effect can be mathematically explained from Bode integral theorem in terms of integral inequalities imposed on the closed-loop transfer function. According to the Bode sensitivity theorem, the sensitivity constraint (Freudenberg *et al.*, 1985) is given by,

$$\int_0^\infty \log |S(j\omega)| d\omega = \pi \sum_{i=1}^{N_p} \text{Re}(p_i) = c \tag{16}$$

where  $c$  is a positive constant, depending upon the number ( $N_p$ ) of ORHP poles ( $p_i$ ).

With a minimum phase system, the area of sensitivity reduction, where  $\log|S(j\omega)|$  is negative, i.e.  $|S(j\omega)| < 1$ , is equal to the area of sensitivity increase, where  $\log|S(j\omega)|$  is positive, i.e.  $|S(j\omega)| > 1$  (Bode *et al.*, 1945; Doyle *et al.*, 1992). Under the ORHP pole ( $p_i$ ), the  $\log|S(j\omega)|$  in Equation 16 indicates a greater area of amplification than attenuation. Hence, the achievable performance is degraded. The performance limitation can also be demonstrated using the time domain simulation to explore the machine terminal voltage response. The time responses in Figure 7 are plotted with (solid line) and without (dashed line) the ORHP pole. Both are stable under excitation control. However, the time response (solid line) obviously settles at a higher value than

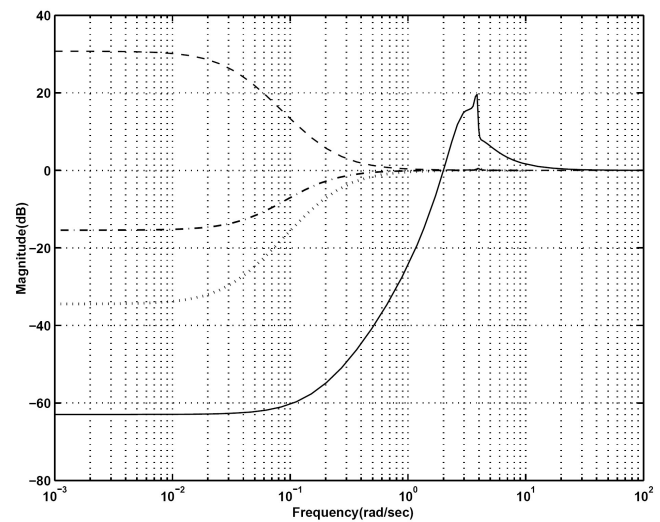


Figure 6. Sensitivity functions (dotted line; 5% below 1.087104pu, without excitation dashed-dotted line; 5% above 1.087104pu, without excitation dashed line; 10% above 1.087104pu, without excitation solid line; 10% above 1.087104pu, with excitation control)

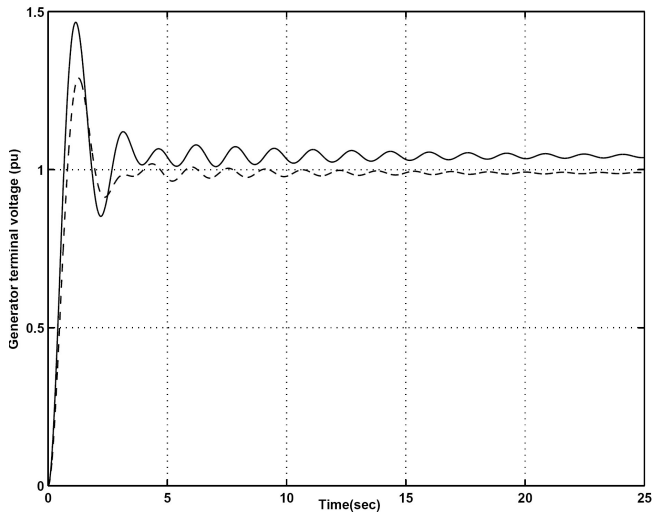


Figure 7. Time responses of generator terminal voltage under excitation control (dashed line; 5% below 1.087104pu, solid line; 10% above 1.087104pu)

the set point (1.0 pu). Therefore, the ORHP pole limits the achievable performance of excitation control. In addition, an unavoidable transient overshoot in the time response is observed in relation to the high frequency sensitivity peak, as seen in Figure 6 (solid line).

The study is further carried out using the sensitivity function to demonstrate the limitation in operating gain ( $K_a$ ) of exciter under ORHP pole. The sensitivity function plots with various gains are shown in Figure 8. When  $K_a$  is increased, an improvement of the low-frequency disturbance rejection is observed together with an increased area of disturbance amplification, which is shifted to the higher frequency region. The sensitivity peaks are highly pronounced at  $\omega_1=3.21$ ,  $\omega_2=4.08$ , and  $\omega_3=9$  rad/sec, with making use of

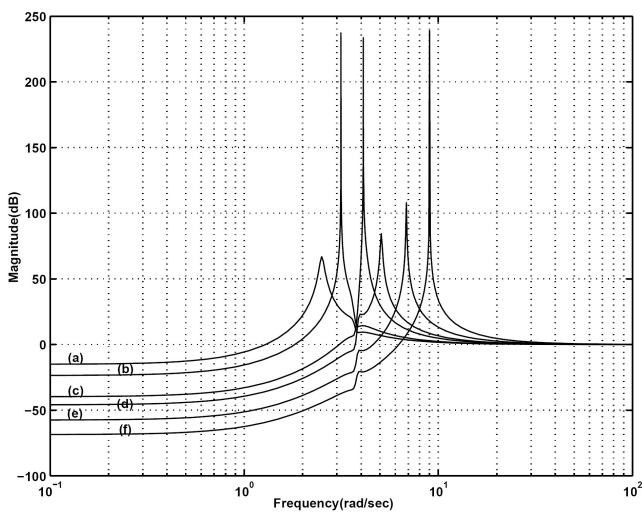


Figure 8. Sensitivity functions (a;  $K_a=10$ , b;  $K_a=13.63$ , c;  $K_a=26.54$ , d;  $K_a=35$ , e;  $K_a=60$ , f;  $K_a=101.8$ )

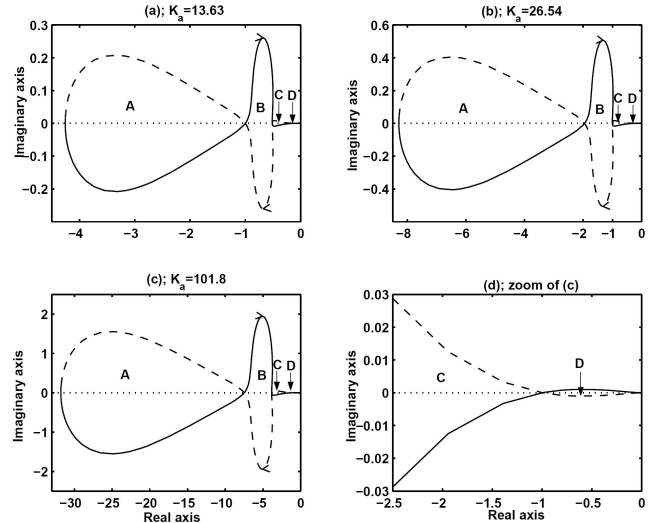


Figure 9. Nyquist plots with various exciter gains

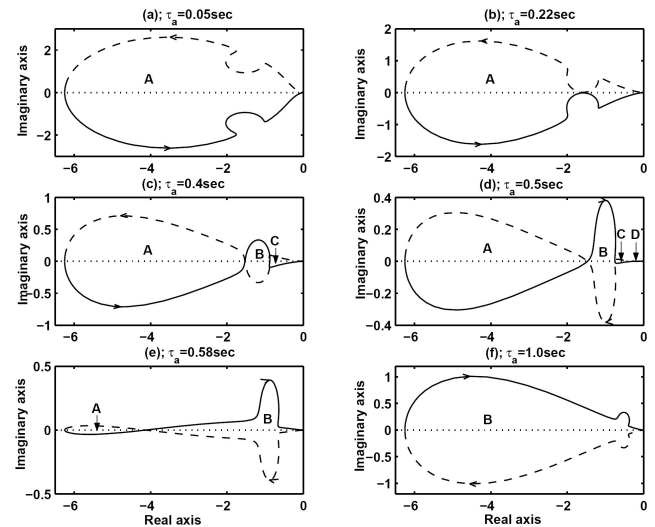


Figure 10. Nyquist plots with various exciter time constants

$K_a=13.63$ ,  $26.54$ , and  $101.8$ , respectively. At these frequencies, the closed-loop instability occurs because of large disturbance amplification. The instability with these gains can be explored using the Nyquist diagram of the open-loop transfer function  $\Delta E/\Delta e$ , as shown in Figure 9. Four stability regions exist (A, B, C, and D), because the Nyquist diagram crosses the  $-180^\circ$  axis three times. As  $K_a$  is increased, the diagram is shifted towards the left, with an increased gain crossover frequency and steady-state gain, without changing in the phase characteristics. If the  $(-1, j0)$  point falls into the regions A and C, the system is closed-loop stable because the Nyquist diagram encircles the  $(-1, j0)$  point one time counter clockwise. On the other hand, if the  $(-1, j0)$  point falls into the regions B ( $13.63 < K_a < 26.54$ ) and D ( $K_a \geq 101.8$ ), the stability is lost. It is clearly shown that the ranges of gain are limited for the stability conditions. For example, a decrease of  $K_a$  below 26.54 or an increase of  $K_a$  above 101.8

can destabilize the system. Hence, the choice of gain to achieve a good control performance is more difficult.

Moreover, it is of interest to explore the stability regions through the Nyquist diagram, when the exciter time constant ( $\tau_a$ ) is varied. Figure 10 shows significant changes in phase characteristics of the Nyquist diagram as  $\tau_a$  is increased from 0.05 to 1 sec with  $K_a$  at 20. With a small value of  $\tau_a$  (0.05), the system is unconditionally stable with a region A. When  $\tau_a$  is raised up to 0.4 sec, the dip in phase occurring in the neighborhood of the electromechanical oscillation frequency does go below the  $-180^\circ$  axis and returns, producing the three regions A, B, and C. The region D at higher frequency ranges also appears with an increased time constant of 0.5 sec. Under this circumstance, the system is conditionally stable. Finally, the system is undoubtedly unstable for all exciter gains with  $\tau_a=1$  sec, since the system phase is entirely below the  $-180^\circ$  axis. Based on these results, the system is stable only for limited ranges of gain and time constant.

## 6. Conclusions

The fundamental studies in this paper show that the mechanism of excitation control system can be related to the main interaction between the synchronous machine flux linkages and the intermediate load. An increase in the intermediate load can cause a significant change in the open-loop characteristic of the flux linkage channel ( $\Delta E'_q / \Delta E_f$ ) from minimum to non-minimum phase, resulting in the non-oscillatory instability of the power system with synchronous machines under the manual excitation. The non-minimum phase change of  $\Delta E'_q / \Delta E_f$  relates to a great amplification of low frequency sensitivity. However, if the machines were under the excitation control, the stability would be maintained under the non-minimum phase condition because the closed-loop poles are moved from the right- to left-half plane by the excitation control feedback. The fundamental studies also indicate a poor feedback performance with an inevitable increase in the area of disturbance amplification at some frequency ranges under the non-minimum phase condition, regarding the ORHP pole. The ORHP pole produces the negative error that causes a rise in the terminal voltage above the set point value. In addition, the study demonstrates the conditional stability of excitation control system, in which its stability can be destabilised by an increase or decrease of the exciter gain. Hence, the exciter gain is limited for a certain range for stability condition.

## References

- Anderson, P. M. and Fouad, A. A. 1993. Power system control and stability, IEEE Press, New York, U.S.A., pp. 440.
- Arrillaga, J. and Arnold, C. P. 1990. Computer analysis of power system, John Wiley & Sons, England, pp. 158-163.
- Aree, P. 2006. Effects of intermediate load on damping of synchronous generator. European Transactions on Electrical Power. 16, 379-392.
- Bode, H. 1945. Network analysis and feedback amplifier design, Van Nostrand Reinhold, New York, U.S.A.
- Crow, M. L. and Lesieutre, B. C. 1994. Voltage collapse. IEEE Potential. 13, 18-21.
- Demello, F. P. and Concordia, C. 1969. Concepts of synchronous machine stability as affected by excitation control. IEEE Transactions on Power Apparatus and Systems. 88, 316-327.
- Doyle, J. C., Francis, B. A. and Tannenbaum, A. R. 1992. Feedback Control Theory, Macmillan, New York, U.S.A.
- Freudenberg, J. S. and Loze, D. P. 1985. Right half plane pole and zeros and design tradeoffs in feedback system. IEEE Transactions on Automatic Control. 30, 555-565.
- Gebreselassie, A. and Chow, J. H. 1994. Investigation of the effects of load models and generator voltage regulators on voltage stability. International Journal of Electrical Power and Energy Systems. 16, 83-89.
- Hajagos, L. 2003. An update on power system stabilization via excitation control. IEEE Power Engineering Society General Meeting, 3, 13-17.
- Huang, H. P. and Chen, C. C. 1997. Control-system synthesis for open-loop unstable process with time delay. IEE Proceedings Control Theory and Applications. 144, 334-346.
- IEEE Task Force. 1993. Load representation for dynamic performance analysis. IEEE Transactions on Power Systems. 8, 472-482.
- Kao, W. 2001. Effect of load models on unstable low-frequency oscillation damping in Taipower system experience with and without power system stabilizers. IEEE Power Engineering Review. 21, 72-72.
- Kundur, P. 1993. Power system stability and control, McGraw-Hill, New York.
- Milanovic, J. V. and Hiskens, I. A. 1995. Effects of load dynamics on power system damping. IEEE Transactions on Power Systems. 14, 1022-1028.
- Padiyar, K. R. 1995. Power system dynamics stability and control, John Wiley & Sons, New York, U.S.A.
- Wu, C., Chang, W. and Cheng, C. 1999. Enhancement of static excitation system performance for generators near electric arc furnace loads. IEEE Transactions on Energy Conversion. 14, 225-231.
- Zhao, Q. and Jiang, J. 1995. Robust controller design for generator excitation system. IEEE Transactions on Energy Conversion. 10, 201-209.

**Appendix A**

Electrical power

$$K_1 = -(E'_d + (X'_d - X'_q)I_q) \frac{V_\infty}{X_{t1}} \left( \frac{B_q \sin \delta + G_q \cos \delta}{B_d B_q + G_d G_q} \right) + (E'_q + (X'_d - X'_q)I_d) \frac{V_\infty}{X_{t1}} \left( \frac{B_d \cos \delta - G_d \sin \delta}{B_d B_q + G_d G_q} \right) \tag{A-1}$$

$$K_{2q} = I_q - (E'_d + (X'_d - X'_q)I_q) \left( \frac{G_q G_L - B_q (B_L - 1/X_{t1})}{B_d B_q + G_d G_q} \right) + (E'_q + (X'_d - X'_q)I_d) \left( \frac{G_L}{B_d B_q + G_d G_q} \right) \tag{A-2}$$

$$K_{2d} = I_d + (E'_q + (X'_d - X'_q)I_d) \left( \frac{G_d G_L - B_d (B_L - 1/X_{t1})}{B_d B_q + G_d G_q} \right) + (E'_d + (X'_d - X'_q)I_q) \left( \frac{G_L}{B_d B_q + G_d G_q} \right) \tag{A-3}$$

$$K_{1G} = -(E'_d + (X'_d - X'_q)I_q) V_L \left( \frac{B_q \sin(\delta - \theta) + G_q \cos(\delta - \theta)}{B_d B_q + G_d G_q} \right) + (E'_q + (X'_d - X'_q)I_d) V_L \left( \frac{B_d \cos(\delta - \theta) - G_d \sin(\delta - \theta)}{B_d B_q + G_d G_q} \right) \tag{A-4}$$

$$K_{1B} = (E'_d + (X'_d - X'_q)I_q) V_L \left( \frac{B_q \cos(\delta - \theta) - G_q \sin(\delta - \theta)}{B_d B_q + G_d G_q} \right) + (E'_q + (X'_d - X'_q)I_d) V_L \left( \frac{B_d \sin(\delta - \theta) + G_d \cos(\delta - \theta)}{B_d B_q + G_d G_q} \right) \tag{A-5}$$

where,

$$B_q = 1 - (B_L - 1/X_{t1})(X_{t2} + X'_q) \tag{A-6}$$

$$B_d = 1 - (B_L - 1/X_{t1})(X_{t2} + X'_d) \tag{A-7}$$

$$G_q = G_L(X_{t2} + X'_q) \tag{A-8}$$

$$G_d = G_L(X_{t2} + X'_d) \tag{A-9}$$

D-axis flux linkage

$$K_{3q} = \frac{G_d G_q + B_d B_q}{G_D G_q + B_D B_q} \quad (\text{A-10})$$

$$K_{4q} = (X_d - X'_d) \frac{V_\infty}{X_{t1}} \left( \frac{B_q \sin \delta + G_q \cos \delta}{G_D G_q + B_D B_q} \right) \quad (\text{A-11})$$

$$K_{7q} = (X_d - X'_d) \left( \frac{G_L}{G_D G_q + B_D B_q} \right) \quad (\text{A-12})$$

$$K_{2G} = (X_d - X'_d) V_L \left( \frac{B_q \sin(\delta - \theta) + G_q \cos(\delta - \theta)}{G_D G_q + B_D B_q} \right) \quad (\text{A-13})$$

$$K_{2B} = (X_d - X'_d) V_L \left( \frac{B_q \cos(\delta - \theta) - G_q \sin(\delta - \theta)}{G_D G_q + B_D B_q} \right) \quad (\text{A-14})$$

where,

$$G_D = G_L (X_{t2} + X_d) \quad (\text{A-15})$$

$$B_D = 1 - (B_L - 1/X_{t1})(X_{t2} + X_d) \quad (\text{A-16})$$

Q-axis flux linkage

$$K_{3d} = \frac{G_d G_q + B_d B_q}{G_d G_Q + B_d B_Q} \quad (\text{A-17})$$

$$K_{4d} = (X_q - X'_q) \frac{V_\infty}{X_{t1}} \left( \frac{B_d \cos \delta - G_d \sin \delta}{G_d G_Q + B_d B_Q} \right) \quad (\text{A-18})$$

$$K_{7d} = (X_q - X'_q) \left( \frac{G_L}{G_d G_Q + B_d B_Q} \right) \quad (\text{A-19})$$

$$K_{3G} = (X_q - X'_q) V_L \left( \frac{B_d \cos(\delta - \theta) - G_d \sin(\delta - \theta)}{G_d G_Q + B_d B_Q} \right) \quad (\text{A-20})$$

$$K_{3B} = (X_q - X'_q) V_L \left( \frac{B_d \sin(\delta - \theta) + G_d \cos(\delta - \theta)}{G_d G_Q + B_d B_Q} \right) \quad (\text{A-21})$$

where,

$$G_Q = G_L (X_{t2} + X_q) \quad (\text{A-22})$$

$$B_Q = 1 - (B_L - 1/X_{t1})(X_{t2} + X_q) \quad (\text{A-23})$$

Generator terminal voltage

$$K_5 = -\frac{E_{tq}}{E_t} \frac{X'_d}{X_{t1}} V_\infty \left( \frac{B_q \sin \delta + G_q \cos \delta}{B_d B_q + G_d G_q} \right) - \frac{E_{td}}{E_t} \frac{X'_q}{X_{t1}} V_\infty \left( \frac{B_d \cos \delta - G_d \sin \delta}{B_d B_q + G_d G_q} \right) \quad (\text{A-24})$$

$$K_{6q} = \frac{E_{tq}}{E_t} \left( 1 - X'_d \frac{G_q G_L - B_q (B_L - 1/X_{t1})}{B_d B_q + G_d G_q} \right) - \frac{E_{td}}{E_t} X'_q \left( \frac{G_L}{B_d B_q + G_d G_q} \right) \tag{A-25}$$

$$K_{6d} = \frac{E_{td}}{E_t} \left( 1 - X'_q \frac{G_d G_L - B_d (B_L - 1/X_{t1})}{B_d B_q + G_d G_q} \right) + \frac{E_{tq}}{E_t} X'_d \left( \frac{G_L}{B_d B_q + G_d G_q} \right) \tag{A-26}$$

$$K_{4G} = \frac{E_{tq}}{E_t} X'_d V_L \left( \frac{B_q \sin(\delta - \theta) + G_q \cos(\delta - \theta)}{B_d B_q + G_d G_q} \right) + \frac{E_{td}}{E_t} X'_q V_L \left( \frac{B_d \cos(\delta - \theta) - G_d \sin(\delta - \theta)}{B_d B_q + G_d G_q} \right) \tag{A-27}$$

$$K_{4B} = \frac{E_{tq}}{E_t} X'_d V_L \left( \frac{B_q \cos(\delta - \theta) - G_q \sin(\delta - \theta)}{B_d B_q + G_d G_q} \right) - \frac{E_{td}}{E_t} X'_q V_L \left( \frac{B_d \sin(\delta - \theta) + G_d \cos(\delta - \theta)}{B_d B_q + G_d G_q} \right) \tag{A-28}$$

Load bus voltage

$$K_{v\delta} = \frac{V_\infty}{X_{t1} Det} \left( -G_L \cos(\theta) + (B_L - XX) \sin(\theta) - (X'_d / D_d) \cos(\delta) \sin(\delta - \theta) + (X'_q / D_q) \sin(\delta) \cos(\delta - \theta) \right) \tag{A-29}$$

$$K_{vq} = \frac{G_L \sin(\delta - \theta) - (B_L - XX + X'_q / D_q) \cos(\delta - \theta) + \frac{K_{v\delta}}{V_\infty} \left( G_L + (X'_d / D_d - X'_q / D_q) \sin(\delta - \theta) \cos(\delta - \theta) \right)}{(X'_d + X_{t2}) Det} \tag{A-30}$$

$$K_{vd} = \frac{G_L \cos(\delta - \theta) + (B_L - XX + X'_d / D_d) \sin(\delta - \theta)}{(X'_q + X_{t2}) Det} \tag{A-31}$$

$$\tag{A-32}$$

$$K_{vB} = \frac{V_L}{Det} \left( -(B_L - XX) - (X'_q / D_q) \cos^2(\delta - \theta) - (X'_d / D_d) \sin^2(\delta - \theta) \right) \tag{A-33}$$

where,

$$D_d = X_{t2} (X'_d + X_{t2}) \tag{A-34}$$

$$D_q = X_{t2} (X'_q + X_{t2}) \tag{A-35}$$

$$XX = \frac{X_{t1} + X_{t2}}{X_{t1} X_{t2}} \tag{A-36}$$

$$Det = G_L^2 + (B_L - XX)^2 + \left( (B_L - XX)(X'_q D_d + X'_d D_q) + X'_q X'_d \right) / D_d D_q \tag{A-37}$$